Properties of a sinusoidally driven thermostat

Y. Zhao and G. J. Morales

Properties of a sinusoidally-driven thermostat

Y. Zhao and G. J. Morales

Physics and Astronomy Department, University of California Los Angeles, CA 90095

This analytical and numerical study explores, from a deterministic perspective, the response of a particle in contact with a heat bath to an external force that varies sinusoidally in time. The heat bath is represented as a deterministic Nosé-Hoover thermostat. Such an idealized model encompasses features found in a variety of physical problems in which the coherent influence of an external agent competes against the thermalization tendencies of the surrounding medium, e.g., a charged particle in a thermal plasma that is acted by a powerful electromagnetic wave. It is found that, independently of the coupling strength to the thermostat, average power can only be extracted from the sinusoidal force when the oscillatory velocity exceeds the thermal velocity. It follows from this property that candidate heat baths whose temperature is raised solely through the application of a sinusoidal force (e.g., radio-frequency heating), reach, in a finite time, a unique final temperature determined by the force parameters. The transition boundary separating the two domains of power transfer is shown to be dominated by chaotic behavior. The combined response to a sinusoidal force and a DC force are also considered and the relevant regions of power transfer are delineated.

I.   I. INTRODUCTION

A.

1.

The competition between the coherent response to a sinusoidal force and the randomization associated with the simultaneous coupling to a heat bath is a basic process encountered in a wide variety of physical environments. The topics in which the coherent/thermal competition arises, range broadly from the thermodynamics of a driven colloidal particle [1], to the motion of a charged particle in a thermal plasma that is irradiated by a powerful electromagnetic wave.

Many of the key underlying issues in this general area, and the seeds for numerous applications, can be traced to Kramers' pioneering study [2] of Brownian motion in a field of force and the diffusion model of chemical reactions. The basic concepts related to the ergodic properties of Brownian motion of a particle exposed to external periodic modulations have been elucidated by Jung and Haenggi [3] using methods based on stochastic differential equations. Goychuck et al. [4] explored the possibility of controlling electron transfer rates in condensed media by studying the coupling to a heat bath of a two-level system driven by a strong periodic field. Sinusoidal forcing of an oscillator in contact with a thermostat was investigated experimentally by Dourche et al. [5] and found to result in surprising time responses that were explained in terms of work fluctuation theorems. Van Zon and Cohen [6] found that an extension of the fluctuation theorem to a system with deterministic and stochastic components indicates that, for large fluctuations, the particles absorb rather than supply heat. The competition and cooperation between thermal noise and a external driving force have been investigated by Bao et al. [7] to demonstrate the transport properties of a particle in a flashing ratchet. Guantes and Miret-Artes [8] combined deterministic chaotic dynamics driven by a periodic force with a model of Gaussian noise to demonstrate the active control of self-diffusion. Significantly, at the present time there is much excitement among condensed matter researchers to explore new phases of matter made possible by the periodic driving of thermal quantum systems [9] and the associated concept of time-crystals [10].

Motivated by the many applications and the vigorous activity surrounding this subject, the present investigation explores some of the simplest non-trivial questions that arise when the coherent/thermal competition is viewed from a deterministic perspective. For example, what is the response of a particle in contact with a deterministic thermostat when an external sinusoidal force is applied? Are there hidden resonances due to the nonlinear coupling to the heat bath? Does the particle extract energy from the sinusoidal driver for all frequencies? What is the role of large amplitude drivers? How does the energy extracted modify the thermostat? Are there chaotic regimes of behavior?

To obtain concrete answers to the previous questions, the present study uses the simplest deterministic thermostat, namely the Nosé-Hoover model [11-14], based on Hamiltonian dynamics. Future, detailed investigations guided by the results obtained in the present study should consider more elaborate thermostat models [15, 16]. For completeness, it should be mentioned that Esposito and Monnai [17] previously studied the connection between nonequilibrium thermodynamics and the Nosé-Hoover thermostat by considering the correlations that arise between the system-reservoir under external forcing.

The major feature identified in this study is the key role played by the ratio of the average oscillatory velocity to the thermal velocity, i.e., $F/\sqrt{2}m\overline{v}\omega$, where F is the amplitude of the sinusoidal force having angular

frequency ω, m is the mass of the particle, and $\overline{v}$ the corresponding thermal velocity. It is found that, independently of the coupling strength to the thermostat, average power can only be extracted from the sinusoidal force when the oscillatory velocity exceeds the thermal velocity. It has been concluded from this property that candidate heat baths whose temperature is raised solely through the application of a sinusoidal force (e.g., radio-frequency heating), reach, in a finite time, a unique final temperature determined by the force parameters. The transition boundary separating the two domains of power transfer is found to be dominated by chaotic behavior.

The manuscript is organized as follows. Section II describes the basic equations of the model and reviews the relevant aspects of the Nosé-Hoover thermostat that impact the present investigation. Section III implements approximate analytic descriptions that capture the major features of the underlying dynamics. Numerical results are presented in Sec. IV and comparisons are made to the analytic predictions. Conclusions are given in Sec.V.

II.   II. FORMULATION

To provide a reference point for the exploration of the sinusoidally-driven system it is first useful to review the properties of a free particle interacting with a classic Nosé-Hoover thermostat [11-14]. The equation of motion for a particle with mass m and velocity v in one-dimension, and the time variable denoted by t, is

$$m\frac{dv}{dt} = -\gamma(t)mv, \qquad (1)$$

with γ the self-consistent damping coefficient representing the coupling to the heat bath, and evolving according to

$$\frac{d\gamma}{dt} = t_0^{-2}\left[\left(\frac{v}{\overline{v}}\right)^2 - 1\right], \qquad (2)$$

where t_0 is the effective coupling time between the particle and the reservoir, and $\overline{v}$ the thermal velocity. The natural scaling of this system results in the scaled variables used later in the numerical study,

$$u = \frac{v}{\overline{v}}, \ \tau = \frac{t}{t_0}, \ \Gamma = \gamma t_0, \ \eta = \frac{x}{\overline{v}t_0}, \qquad (3)$$

in which x is the physical position (e.g. in cm) and η the scaled position. The corresponding scaled, dynamical system becomes

$$\frac{du}{d\tau} = -\Gamma u, \qquad (4)$$

$$\frac{d\Gamma}{d\tau} = u^2 - 1. \qquad (5)$$

This simple system has three built-in constraints: two conserved quantities, and the preservation of the initial
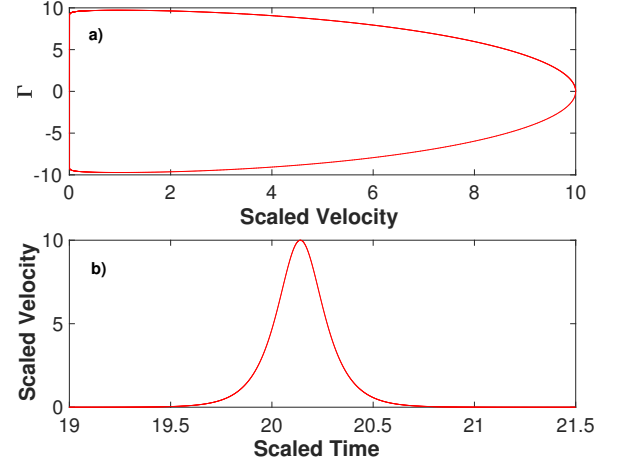

FIG. 1. Behavior of an initially fast particle with $u(\tau = 0) = 10$ interacting with the heat reservoir. Top panel a) shows the scaled phase-space orbit (Γ, u), and bottom panel b) the temporal evolution of the scaled velocity. Only one pulse from the periodic orbit is shown. Γ is the scaled damping coefficient and u the scaled velocity, as given by Eq. (3).

sign of the scaled velocity u. The conserved quantities U_0 and K take the form

$$K = u\exp\theta; \ \theta = \int d\tau \Gamma(\tau), \qquad (6)$$

and

$$U_0 = \frac{u^2}{2} + \frac{\Gamma^2}{2} + \theta. \qquad (7)$$

The associated nonlinear orbits are closed in the (Γ, u) phase-space with a scaled period τ_p given by

$$\tau_p = 2\int_0^{u_t} \frac{du}{u\sqrt{2U_0 - u^2 + 2\ln(u/K)}}, \qquad (8)$$

where u_t is the turning velocity corresponding to the zero of the square root.

The simplest orbit corresponds to sinusoidal oscillations about the fixed point at $u = \pm 1$; it has a scaled angular frequency $w_0 = \sqrt{2}$. For initial velocities u_0 significantly different from $|1|$, the orbits consist of periodic pulses with algebraically decaying tails (faster than Lorentzian). Figure 1 illustrates the typical behavior for an initially fast particle with $u_0 = 10$. The top panel displays the (Γ, u) phase-space trajectory and the bottom panel exhibits the temporal behavior of the scaled velocity; only one pulse is shown. What is remarkable about this simple thermostat model is that, independently of the initial conditions, the time–average of the scaled squared velocity is 1, i.e., $\langle v^2 \rangle = \overline{v}^2$. For the particular orbit shown in Fig. 1 it is seen that this thermalization is achieved by the particle spending most of the time at very small velocities and punctuated by short flights through the large velocity intervals.
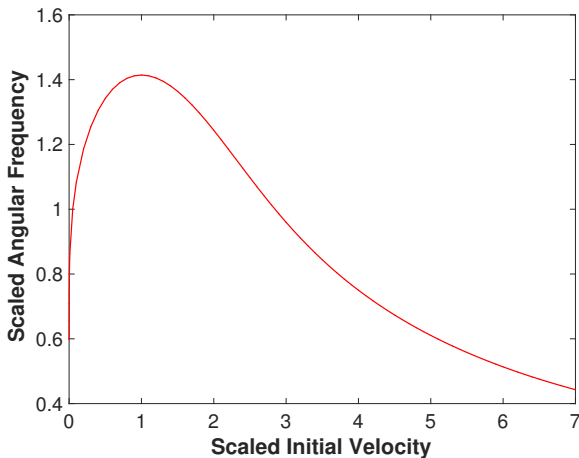
FIG. 2. Dependence of the scaled, angular frequency of nonlinear periodic orbits on initial scaled velocity $u(\tau = 0)$. The highest frequency corresponds to $w_0 = \sqrt{2}$, associated with sinusoidal oscillations about the thermal velocity, i.e., $v = \overline{v}$. Note that this is not the frequency of the external force presented in other figures.

Figure 2 illustrates the dependence of the scaled angular frequency of oscillation on the initial scaled velocity obtained from Eq. (8), and also verified from direct numerical solution of Eqs. (4) and (5). It is seen that the largest frequency corresponds to the linear oscillations about the fixed point, i.e., $\sqrt{2}$. This figure also provides a useful reference for results presented later in which the frequency of the external driver is varied.

The simplest external perturbation to a free particle in contact with the heat reservoir consists of the application of a constant (DC) force F_0. This is also of relevance to the present study since it corresponds to the special case in which the frequency of the sinusoidal driver is zero. The response to the DC force is simple: every particle, regardless of its initial velocity, quickly settles to a velocity equal to the thermal velocity. The stationary point has the scaled values $u = 1$, $\Gamma = f_0$, where $f_0 = \frac{F_0 t_0}{m\overline{v}}$ is the scaled DC force. Small perturbations in Γ and u about this point exhibit a characteristic response proportional to $\exp(s\tau)$ with s the complex frequency given by

$$s = -\frac{f_0}{2} \pm \frac{\sqrt{f_0^2 - 8}}{2}. \qquad (9)$$

In the limit of vanishing DC force Eq. (9) recovers the oscillations about the thermal velocity at a scaled frequency $w_0 = \sqrt{2}$. This Eq. also gives an example, for the simple orbits close to the thermal velocity, of how an external force destroys (here for $f_0 > \sqrt{8}$) the periodic energy exchange between a particle and the heat reservoir. Analogous, but more complex modifications are also at work for particles of arbitrary initial velocity; the consequence is the destruction of the periodic, pulsed

orbits of the type shown in Fig 1. The steady power delivered by the DC force is $P_0 = F_0 \overline{v}$, independently of the coupling strength between the particle and the thermostat. The particle acts as a mediator that transfers this power from the source of the force to the reservoir.

Next the effect of a sinusoidal force $F \sin(\omega t)$ is considered. The scaled dynamical Eq. (4) becomes

$$\frac{du}{d\tau} = A \sin(w\tau) - \Gamma u, \qquad (10)$$

where $A = \frac{F t_0}{m\overline{v}}$ is the scaled amplitude of the AC force and $w = \omega t_0$ is the corresponding scaled angular frequency.

III.   III. APPROXIMATE DESCRIPTION

In this section approximate analytic solutions of Eqs. (10) and (5) are considered. Predictions extracted from these approximations are later compared in Sec. IV to the numerical solutions.

The starting point in the approximation scheme is the ansatz that $\Gamma = \langle \Gamma \rangle + \delta\Gamma$, in which $\langle \Gamma \rangle$ is time-independent, and $\delta\Gamma$ is a small fluctuating quantity that in lowest-order does not contribute significantly to the strong constraint posed by the thermostat, namely that $\langle u^2 \rangle = 1$. The concept is to solve for the time-dependent, scaled velocity u assuming that $\langle \Gamma \rangle$ is known. Then by demanding that $\langle u^2 \rangle = 1$, the self-consistent value of $\langle \Gamma \rangle$ is determined. Once this information is known, the solution for $\delta\Gamma$ can be obtained by iteration. The procedure yields the time evolution of the (Γ, u) phase-space orbit, and the average power transferred from the sinusoidal force to the system. The implementation of this logic results in

$$u = -\sqrt{2} \cos(w\tau + \theta), \qquad (11)$$

$$\delta\Gamma = \frac{1}{2w} \sin(2w\tau + 2\theta), \qquad (12)$$

$$\tan\theta = \frac{\langle \Gamma \rangle}{w}, \qquad (13)$$

$$\langle \Gamma \rangle = \sqrt{\frac{A^2}{2} - w^2}, \qquad (14)$$

with the corresponding scaled, average power transferred $\langle P_s \rangle = \langle \Gamma \rangle$. It is seen from Eq. (14) that power transfer is expected to occur only for sufficiently large force amplitudes such that $A > \sqrt{2}w$ (this feature is later assessed in Figs. 3-5). Physically, this corresponds to the average sloshing velocity, or oscillatory velocity driven by the sinusoidal force, being larger than the thermal velocity. From Eqs. (11) and (12) it is deduced that the phase-space trajectory is closed, and has a characteristic

number-eight-shape (this property is later examined in Fig. 6). In the net power-transfer regime the sloshing velocity of the particle is independent of the amplitude of the applied force; its time-average is always equal to the thermal velocity.

In terms of explicit physical parameters, the average power transferred takes the form

$$\langle P \rangle = \omega T \left[\frac{F^2}{2m\omega^2 T} - 1 \right]^{1/2}, \qquad (15)$$

in which T is the temperature of the reservoir (in eV). It is also the case that for the sinusoidal force, the power transfer is independent of the coupling strength to the reservoir. In the limit of very large forces, or low temperatures, Eq.(15) reduces to $\langle P \rangle \rightarrow F\bar{v}/\sqrt{2}$, which is analogous to the result obtained for a DC force, but with the strength of the force now replaced by the appropriate RMS value.

Because of the seemingly universal form of Eq. (15) it is instructive to ask: what would be the behavior if the reservoir itself were to be heated by the action of the external AC force? Clearly, from Eq. (15) there is a maximum temperature

$$T_f = \frac{F^2}{2m\omega^2}, \qquad (16)$$

beyond which the external force does not energize the reservoir. Assuming that the reservoir has a heat capacity C, and that there are N-particles driven by the AC force that are coupled to the reservoir, then the temperature evolves according to

$$C\frac{dT}{dt} = N\omega T \sqrt{\frac{T_f}{T} - 1}. \qquad (17)$$

Defining the scaled temperature ξ and a new, slow scaled-time ψ as

$$\xi = \frac{T}{T_f}, \ \psi = \frac{N\omega t}{C}, \qquad (18)$$

yields

$$\psi(\xi) = \int_0^\xi \frac{ds}{\sqrt{s(1-s)}}, \qquad (19)$$

in which s is now a dummy variable, and whose solution is

$$\xi = \sin^2\left(\frac{\psi}{2}\right). \qquad (20)$$

This result implies that the action of an external sinusoidal force can bring the reservoir to the final temperature T_f in a finite time $t_f = \pi C/N\omega$, independently of the amplitude of the force, and of the coupling strength to the reservoir.

It is worth mentioning that if the free particle also experiences an additional drag force $F_d = -\nu m v$, with ν the constant drag coefficient, and unrelated to the heat reservoir, then the power extracted from the sinusoidal force remains unchanged, i.e., it is given by Eq. (15). The reservoir adjusts by decreasing the value of $\langle \Gamma \rangle$ by an amount νt_0. The consequence is that the reservoir receives less power from the sinusoidal force, and accordingly the final temperature that it could attain, if energized by coupling through N-particles, is reduced, i.e.,

$$T_f \rightarrow \frac{T_f}{1 + \left(\frac{\nu}{\omega}\right)^2}. \qquad (21)$$

The approximation methodology used in obtaining the results summarized in Eqs. (11)-(15) can be extended to incorporate an arbitrary number of sinusoidal forces, each having scaled amplitude A_j and scaled frequency w_j. The increased complexity is that now $\langle \Gamma \rangle$ admits the mathematical possibility of achieving multiple values resulting from the thermalization condition $\langle u^2 \rangle = 1$, which takes the form

$$\sum_j \frac{A_j^2/2}{w_j^2 + \langle \Gamma \rangle^2} = 1, \qquad (22)$$

and with the scaled, average power transferred from all the oscillating forces still being given by $\langle P_s \rangle = \langle \Gamma \rangle$.

For the case of two oscillating forces, Eq. (22) can be solved in closed form to obtain

$$\langle \Gamma \rangle^2 = \frac{1}{2}\left\{ (x_1 + x_2) \pm \left[(x_1 - x_2)^2 + \frac{A_1^2 A_2^2}{4} \right]^{1/2} \right\}, \qquad (23)$$

where

$$x_j = \frac{A_j^2}{2} - w_j^2, \text{ for } j = 1, 2, \qquad (24)$$

and from which only the plus sign yields a real, physical root. The effect of an additional oscillatory force is to increase the frequency domain over which a net transfer of power can be achieved for a fixed amplitude. Physically, this behavior can be interpreted as a boosting of the total sloshing velocity by the second force. This feature is made more transparent by deducing from Eq. (22) what is the threshold frequency beyond which the particle does not extract energy from the forces, i.e., $\langle \Gamma \rangle = 0$. Referencing the parameters of the second oscillatory force in terms of the first by $A_2 = \alpha A_1$, and $w_2 = \beta w_1$, yields the threshold frequency

$$w_{th} = A_1 \sqrt{\frac{1 + (\alpha/\beta)^2}{2}}, \qquad (25)$$

from which it is seen that, for a fixed amplitude, the addition of a second force of much lower frequency, i.e., $\beta \ll 1$, significantly increases the range of frequencies over which the first force can transfer power to the driven particle.

Motivated by this finding it is then natural to explore the extreme case when both a DC force and a sinusoidal force are simultaneously applied. To describe this situation, the ansatz previously made for the behavior of the scaled damping coefficient needs to extended to the scaled velocity, i.e., $u = \langle u \rangle + \delta u$, with $\langle u \rangle$ a time-independent, average velocity to be determined self-consistently, analogous to $\langle \Gamma \rangle$, and δu a fluctuating velocity. The thermalization constraint now becomes

$$\langle (\langle u \rangle + \delta u)^2 \rangle = 1, \qquad (26)$$

from which the unknown $\langle \Gamma \rangle$ is obtained. Again, in this case the same relation for the scaled, total power transferred to the particle is found, i.e., $\langle P_s \rangle = \langle \Gamma \rangle$. And with the clarification that this expression includes the power transferred by the DC force, i.e., $f_0^2/\langle \Gamma \rangle$.

Implementing the outlined procedure results in

$$\langle u \rangle = \frac{f_0}{\langle \Gamma \rangle}, \qquad (27)$$

$$\delta u = - \left[2 \left(1 - \frac{f_0^2}{\langle \Gamma \rangle^2} \right) \right]^{1/2} \cos(w\tau + \theta), \qquad (28)$$

$$\delta \Gamma = -\frac{2}{w} \left[2 \left(1 - \frac{f_0^2}{\langle \Gamma \rangle^2} \right) \right]^{1/2} \langle u \rangle \sin(w\tau + \theta)$$
$$+ \frac{1}{2w} \left[1 - \frac{f_0^2}{\langle \Gamma \rangle^2} \right] \sin(2w\tau + 2\theta), \quad (29)$$

$$\langle \Gamma \rangle^2 = \frac{1}{2} \left(\frac{A^2}{2} + f_0^2 - w^2 \right)$$
$$+ \frac{1}{2} \left[\left(\frac{A^2}{2} + f_0^2 - w^2 \right)^2 + 4w^2 f_0^2 \right]^{1/2}, \quad (30)$$

$$\tan \theta = \frac{\langle \Gamma \rangle}{w}, \qquad (31)$$

where f_0 is the scaled, DC force defined earlier in Sec. II.

Eqs. (28) and (29) indicate that the characteristic number-eight shape of the (Γ, u) phase-space orbit is distorted (stretched in the direction of the force) by the application of the DC force, which by itself would drive the particle towards the fixed point $u = 1$. Eq. (30), analogous to Eq. (23), predicts that the frequency domain over which power can be extracted from the sinusoidal force is increased by the application of the DC force (this behavior is illustrated later in Fig. 12).

The procedure used to obtain the previous approximate results fails for weak oscillatory forces, i.e., $A < \sqrt{2}w$. In this parameter regime the particle orbit is overwhelmingly determined by time-dependent, energy exchanges with the heat bath, i.e., $\langle \Gamma \rangle = 0$ (shown later

in Fig. 9). Now there is a zero-order velocity, $u_0(\tau)$, and a corresponding damping coefficient, $\Gamma_0(\tau)$, of the type illustrated in Fig. 1. The weak external force induces small oscillations δu_w, at scaled frequency w, on both of these quantities. In principle, these oscillations can be calculated by developing a perturbation theory that expands around the (presumably) known nonlinear orbits. The general implementation of such a procedure is lengthy, and the answer a bit unwieldy, and not very useful. In here the simplest case is reported to illustrate the underlying important features. The numerically calculated orbits for this regime are shown later in Sec. IV.

For the case of a particle exhibiting small velocity oscillations about the thermal velocity, with scaled frequency $w_0 = \sqrt{2}$, and scaled damping-coefficient amplitude a,

$$u_0 = 1 + \frac{a}{w_0} \cos(w_0\tau), \; \Gamma_0 = a \sin(w_0\tau). \qquad (32)$$

This yields the equation for the modified velocity

$$\frac{d\delta u}{d\tau} + (a \sin(w_0\tau))\delta u = A \sin(w\tau), \qquad (33)$$

which can be solved exactly to extract the driven oscillation

$$\delta u_w = wA \sum_{n=0}^{\infty} \frac{(-1)^n I_n^2(a)}{(nw_0)^2 - w^2} \cos(w\tau), \qquad (34)$$

with I_n the modified Bessel function of order n. The significant consequence that follows from Eq. (34) is that in this frequency-amplitude regime, $A < \sqrt{2}w$, the external force does not transfer energy to the particle because the response is out-of-phase.

In terms of physical quantities, Eq.(34) yields the generalization of the sloshing velocity induced by an oscillating force to a thermal particle in contact with a deterministic thermostat,

$$v_{osc} \rightarrow \frac{F\omega}{m} \sum_{n=0}^{\infty} \frac{(-1)^n I_n^2(a)}{2 \left(\frac{n}{t_0} \right)^2 - \omega^2}. \qquad (35)$$

Eq. (35) indicates that, in principle, a deterministic thermostat allows for internal thermal resonances when driven externally (this property is illustrated later in Figs. 15 and 16), and also that in the limit $a \rightarrow 0$, the usual free-particle result, leading to the ponderomotive force, is obtained.

The valuable insight extracted from the previous approximate analysis is the identification of a boundary, in the amplitude-frequency space (F, ω), that separates two different domains: one in which power can be extracted, and another in which inertial oscillations modulate the intrinsic thermal motion, without power transfer. However, the assumptions made in the approximate analysis cannot be used to address the issue of what is the width of the transition region across the boundary (this is illustrated later in Figs. 7 and 8). In reality, the boundary is fuzzy and exhibits complex chaotic dynamics that are explored numerically in the following section.
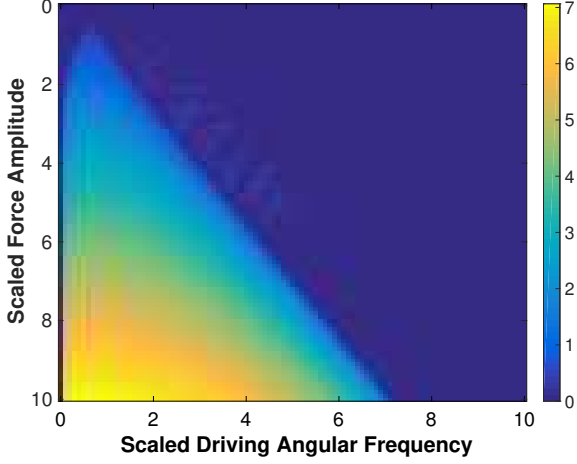
FIG. 3. Color contour of $\langle P_s \rangle$ the scaled, average power extracted from the sinusoidal force, shows the dependencies on the scaled amplitude A and the scaled frequency w. Dark blue represents zero power transfer, and the bright yellow region, large power transfer. A sharp boundary separates these two different power-absorption domains.
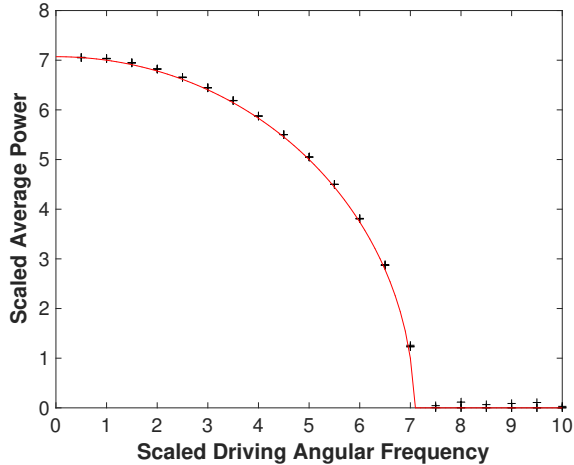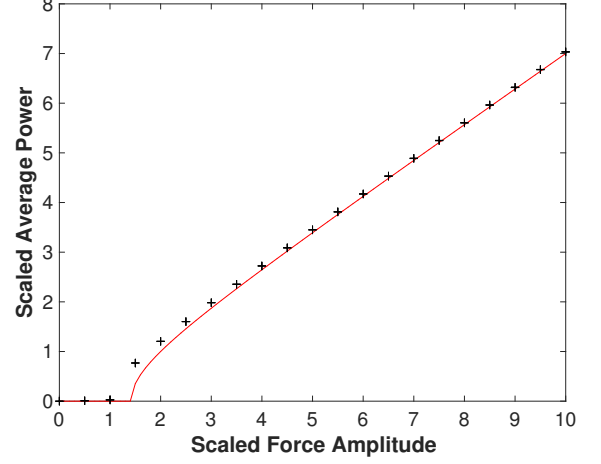

FIG. 5. Line-projection of the color contour of Fig. 3 along a direction of constant scaled frequency, $w = 1$, shows the dependency of $\langle P_s \rangle$ on scaled amplitude. Discrete symbols are the numerical results for three different initial, scaled velocities, $u(\tau = 0) = 10^{-4}$, 0.5, 8. Solid curve is Eq. (14).

FIG. 4. Line-projection of the color contour of Fig. 3 along the direction of constant scaled force, $A = 10$, shows the dependency of $\langle P_s \rangle$ on scaled frequency w. Discrete symbols are the numerical results for three different initial, scaled velocities, $u(\tau = 0) = 10^{-4}$, 0.5, 8. Solid curve is Eq. (14).
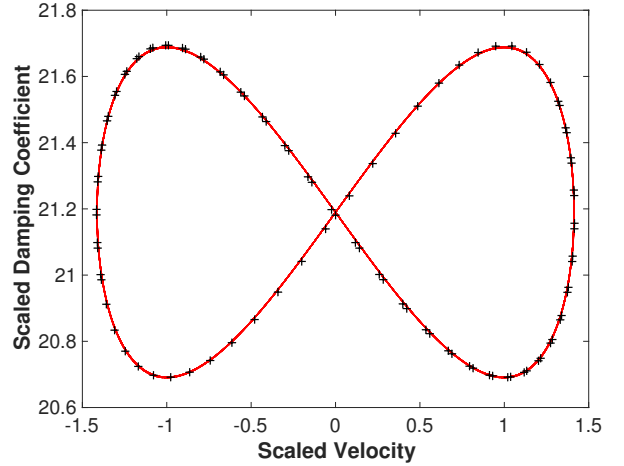

FIG. 6. Characteristic (Γ, u) phase-space orbit for a particle in the power-absorbing domain, $A > \sqrt{2}w$, for a choice of $A = 30$, $w = 1$. Discrete symbols are obtained numerically and the red solid curve is the prediction of Eqs. (11) and (12). Γ is the scaled damping coefficient and u the scaled velocity, as given by Eq. (3). A is the scaled amplitude, defined following Eq. (10).

IV.   IV. NUMERICAL RESULTS

This section presents results obtained by solving the scaled Eqs. (5) and (10) using a fourth-order Runge-Kutta method with a typical time-step $\Delta\tau \leq 10^{-3}$, as is characteristic of studies with the Nosé-Hoover thermostat. All cases reported have an initial reservoir damping $\Gamma(\tau = 0) = 0$.

The color contour display in Fig. 3 corresponds to the scaled, time-average power transferred by the sinusoidal force, $\langle P_s \rangle$, for a wide range of values of the scaled amplitude of the force, A, and the scaled frequency, w. The dark blue region represents zero power transfer from the sinusoidal force, and the bright yellow region, large power transfer. It is evident that a sharp boundary separates these two different power-absorption domains. Barely visible in Fig. 3, there are some faint patches (not fully dark blue) that surround the boundary. These structures actually exhibit small power transfer and are separately examined later in Fig. 7.
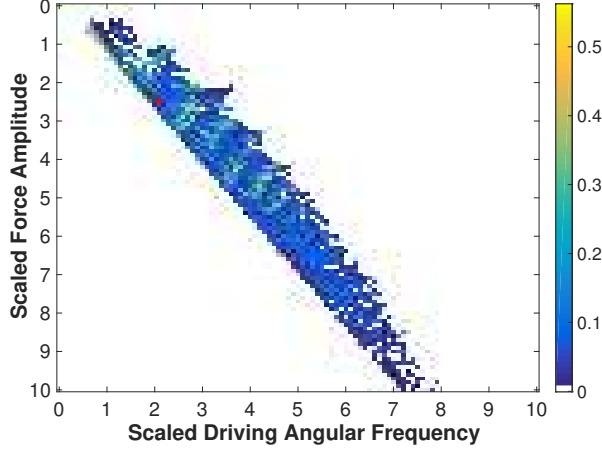
FIG. 7. Enhanced view of the transition region corresponding to the faint patches seen in Fig. 3. To enhance visualization here the dark blue color in Fig. 3 is now white, and all points in the power absorption region are forced to be also white. The power transfer in this transition region is very small, but finite. The red cross is the point chosen for the display in Fig. 8.

Fig. 4 shows a line-projection of the color contour of Fig. 3 along the direction of constant force, $A = 10$, i.e., it illustrates the dependence of $\langle P_s \rangle$ on the scaled frequency. The discrete symbols are the numerical results obtained for three different initial, scaled velocities, $u(\tau = 0) = 10^{-4}$, 0.5, 8, that span a wide range. The solid curve is Eq. (14). The complementary dependency on amplitude, for fixed frequency, $w = 1$, is shown in Fig. 5, with the solid curve again being the prediction of Eq. (14). These comparisons indicate that the predictions of the approximate analysis of Sec. III give a good account of the numerical results. In addition, it is ascertained that the average power transfer is independent of the initial velocity of the particle.

A characteristic (Γ, u) phase-space orbit for a particle in the power-absorbing domain, $A > \sqrt{2}w$, is displayed in Fig. 6 for a choice of $A = 30$, $w = 1$. The discrete symbols are obtained numerically and the solid curve is the prediction of Eqs. (11) and (12). Again, it is seen that the approximate analysis captures well the dynamics in this domain. Note from Fig. 6 that in this domain $\langle \Gamma \rangle \neq 0$ and $\langle u \rangle = 0$, as is assumed in that analysis.

Figure 7 is an enhanced display of the finite transition region separating the two different domains of power absorption identified in Fig. 3. It corresponds to the faint patches in that figure. They are visualized by reversing the color scale, i.e., forcing the dark blue color in Fig. 3 to now be white, and also by arbitrarily setting all points in the power absorption region to be white. In this transition region, of frequency width $\Delta w < w_0 = \sqrt{2}$, the net power absorption is relatively small, but finite. The topology associated with the phase-space orbits is very sensitive to the (A, w) values, and causes the approximate
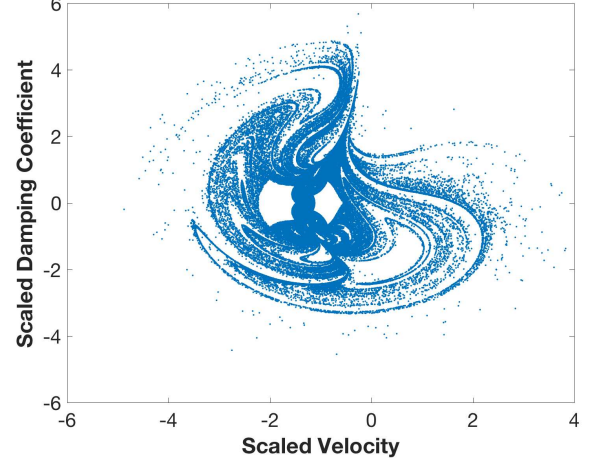

FIG. 8. Poincare map in the (Γ, u) phase-space for the red cross point in the transition region shown in Fig. 7. Sampling time is equal to the period of the sinusoidal force. Γ is the scaled damping coefficient and u the scaled velocity, as given by Eq. (3).
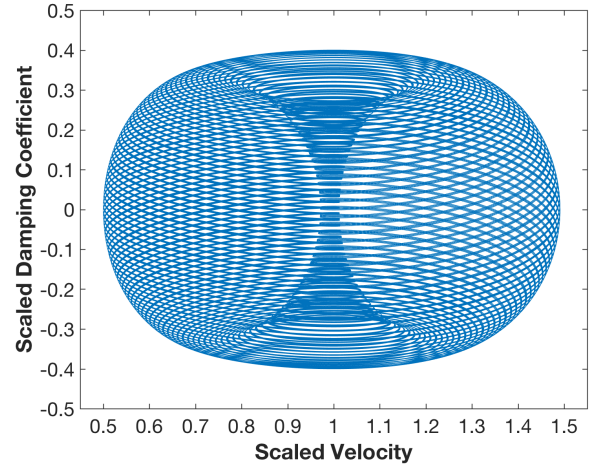

FIG. 9. Typical trajectory in the (Γ, u) phase-space in the domain where no power transfer occurs, $A < \sqrt{2}w$, for $A = 2$, $w = 8$. Here $\langle \Gamma \rangle = 0$, and $\langle u \rangle \neq 0$, as expected from the analysis in Sec. III. Γ is the scaled damping coefficient and u the scaled velocity, as given by Eq. (3). A is the scaled amplitude, defined following Eq. (10).

analysis of Sec. III to fail. Physically, in this transition region the sloshing velocity is equal to the thermal velocity, i.e., the particle is equally influenced by the coherent force and by the heat bath. The resulting effect is that the particle motion displays chaotic behavior.

The rich structure of the chaotic motion in the transition region is illustrated in Fig. 8 for the case $A = 2.5$, $w = 2.1$, corresponding to the red cross in Fig. 7. Shown is a Poincare map for the trajectory in the (Γ, a) phase-space of a particle with initial scaled velocity $u(\tau = 0) = 0.5$, with sampling time equal to the oscillating period of
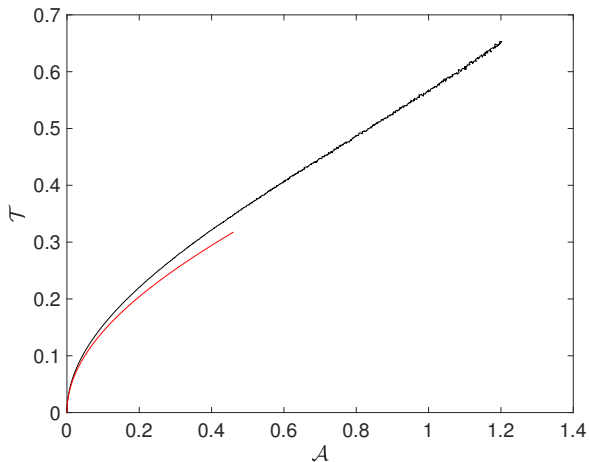
FIG. 10. Path in the $(\mathcal{T}, \mathcal{A})$ Tarnopolski plane for the scaled velocity associated with two cases, as the subsampling scale is increased. The red curve corresponds to a case where there is net power transfer, $(A = 9, w = 1)$, and the black curve to a case in the transition region, $(A = 2.5, w = 2.1)$. The Abbe value $\mathcal{A}$ is one-half of the ratio of the mean square of successive differences to the variance given by Eq. (36). $\mathcal{T}$ is the number of times the derivative attains a zero-value divided by the total number of points in the time series. For a large, random series of numbers its value is $2/3 \approx 0.7$. A is the scaled amplitude, defined following Eq. (10), and w the scaled frequency.

FIG. 11. $(\mathcal{T}, \mathcal{A})$ path followed in the Tarnopolski plane by a particle in the region of zero power transfer for a case $(A = 9, w = 9)$. Reversal of directions in the $(\mathcal{T}, \mathcal{A})$ paths is a manifestation of the competition between two different frequencies, one related to the coupling to the heat bath, and the other to the external force. The Abbe value $\mathcal{A}$ is one-half of the ratio of the mean square of successive differences to the variance given by Eq. (36). $\mathcal{T}$ is the number of times the derivative attains a zero-value divided by the total number of points in the time series. For a large, random series of numbers its value is $2/3 \approx 0.7$. A is the scaled amplitude, defined following Eq. (10), and w the scaled frequency.

the force $2\pi/w$.

A typical trajectory in the (Γ, u) phase-space in the domain where no power transfer occurs, $A < \sqrt{2}w$, is shown in Fig. 9 for a case $A = 2$, $w = 8$. A complex pattern is formed from a mixing of the intrinsic, periodic exchange with the heat bath and the modulation imposed by the sinusoidal force. Note from Fig. 9 that in this case $\langle \Gamma \rangle = 0$, and $\langle u \rangle \neq 0$ as expected from the analysis in Sec. III.

To quantify the nature of the dynamics underlying the behavior in the different domains identified in Figs. 3 and 7, and illustrated by Figs. 6, 8, and 9, the Tarnopolski plane [18] analysis is applied with the perspective illustrated in the study by Zunino et al. [19]. This is a relatively simple methodology that allows the identification of coherent, chaotic, or stochastic dynamics. There are two quantifiers used: the Abbe value $\mathcal{A}$, and the turning-number probability $\mathcal{T}$. The Abbe value is conventionally defined as one-half of the ratio of the mean square successive difference to the variance, i.e., for a discrete sequence of N-numbers x_i with $1 : i : N$

$$\mathcal{A} = \frac{N}{2(N-1)} \frac{\sum_1^{N-1}(x_{i+1} - \overline{x})^2}{\sum_1^N (x_i - \overline{x})^2}, \qquad (36)$$

where $\overline{x}$ is the mean value of the sequence x_i.

$\mathcal{T}$ is simply the fraction of maxima encountered in a given set of discrete points, or alternatively, the number of times the derivative attains a zero-value divided by
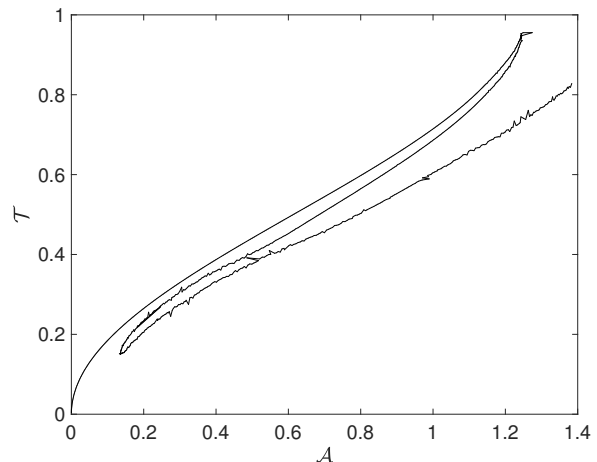
N. For a large, random series of numbers its value is $2/3 \approx 0.7$. As pointed by Zunino et al. [19] for a time series, what is of significance is the path in the $(\mathcal{T}, \mathcal{A})$ plane as the series is sequentially subsampled, so that the various embedded scales are probed.

Fig. 10 shows the path in the $(\mathcal{T}, \mathcal{A})$ plane for the scaled velocity associated with two cases. The red curve corresponds to a case where there is net power transfer, $(A = 9, w = 1)$, and the black curve to a case in the transition region, $(A = 2.5, w = 2.1)$. It is seen that the red curve remains limited to the small $(\mathcal{T}, \mathcal{A})$ values as the scale of the subsampling is increased, implying that the dynamics is coherent, as expected from the analysis in Sec. III. But the black curve corresponding to the transition region increases steadily from the coherent region of small $(\mathcal{T}, \mathcal{A})$ values towards the stochastic region, as the scale of the subsampling is increased. This is the characteristic behavior followed by the classic models of deterministic chaos, as documented previously by Tarnopolski [18] and by Zunino et al. [19], and also anticipated by the Poincare map shown in Fig. 8.

The $(\mathcal{T}, \mathcal{A})$ path followed by a particle in the region of zero power transfer covers a wide range, thus it is displayed separately in Fig. 11. This case corresponds to $(A = 9, w = 9)$. The first leg of the path starting at the origin gives a first impression that this case is another example of deterministic chaos, something that perhaps may be suggested by a blurry look at Fig. 9. But, in fact,
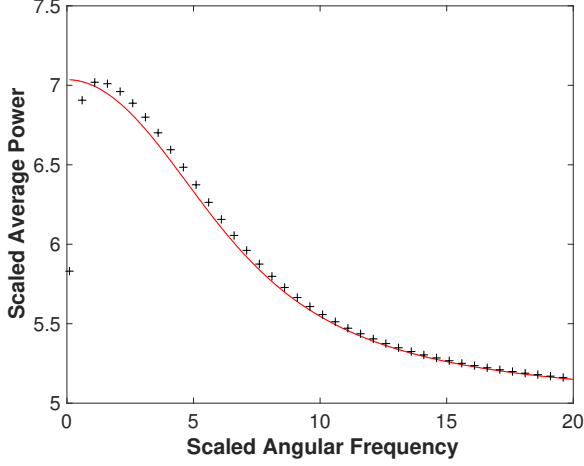
FIG. 12. Situation in which a DC force and an oscillatory force are simultaneously applied. Shown is the frequency dependence of the time-averaged, total power (AC+DC) transferred to the particle, for a fixed value of the DC force and a fixed amplitude of the sinusoidal force; $A = 7$, $f_0 = 5$, $u(\tau = 0) = 0.1$. The solid red curve is the prediction of Eq. (30) and the discrete symbols are the numerical results. A is the scaled amplitude, defined following Eq. (10), and u the scaled velocity.

FIG. 13. Behavior for low-frequency forcing. Shown is time dependence of scaled velocity u for a case $A = 1.95$, $w = 0.09$, and initial velocity $u(\tau = 0) = 0.5$. Long periods of adiabatic balance between the slow, external force and the heat bath are broken by sharp pulses during which the particle acquires several times the thermal energy. Red arrow indicates pulse shown in Fig. 14. A is the scaled amplitude, defined following Eq. (10).

as the subsampling scale is increased the path passes beyond the stochastic value. Further larger subsampling returns the path towards low $(\mathcal{T}, \mathcal{A})$ values, characteristic of coherent dynamics. This reversal of directions in the $(\mathcal{T}, \mathcal{A})$ paths is a manifestation of the competition between two different frequencies, one related to the coupling to the heat bath, and the other to the external force.

Fig. 12 examines the situation in which a DC force and an oscillatory force are simultaneously applied. Shown is the frequency dependence of the time-averaged, total power (AC+DC) transferred to the particle, for a fixed value of the DC force and a fixed amplitude of the sinusoidal force; in this case $A = 7$, $f_0 = 5$, $u(\tau = 0) = 0.1$. The solid red curve is the prediction of Eq. (30) and the discrete symbols are the numerical results. Close agreement is obtained for $w > 5$, corresponding to the region where the sinusoidal force alone does not transfer power. It is seen that the combined effect of the DC and AC forces is to boost the DC-power transfer by an amount $A^2/2$ at the lower frequencies, and to extend the frequency range of AC-power transfer beyond the threshold value, eventually asymptoting for very large frequencies to the pure DC-power transfer $\langle P_s \rangle \to f_0$, or in physical units, $F_0 \overline{v}$. As expected from the comparison shown in Fig. 12, the approximate analysis also reproduces well the phase-space trajectories, within 0.5%, and thus are not shown for brevity.

A surprising behavior appears for low-frequency forcing, in a regime in which the system can be expected to behave adiabatically, i.e., $w \ll 1$. It is found that the
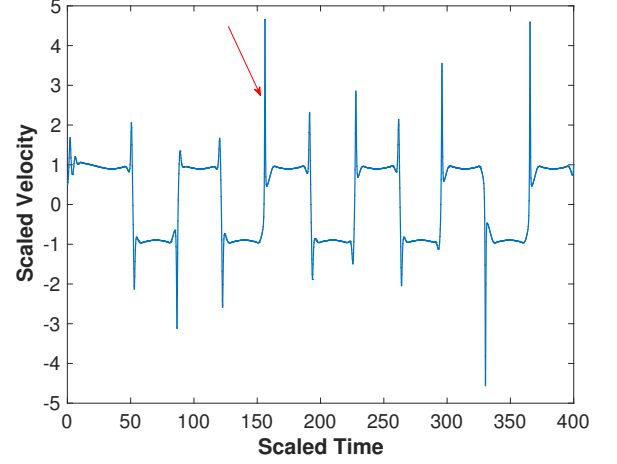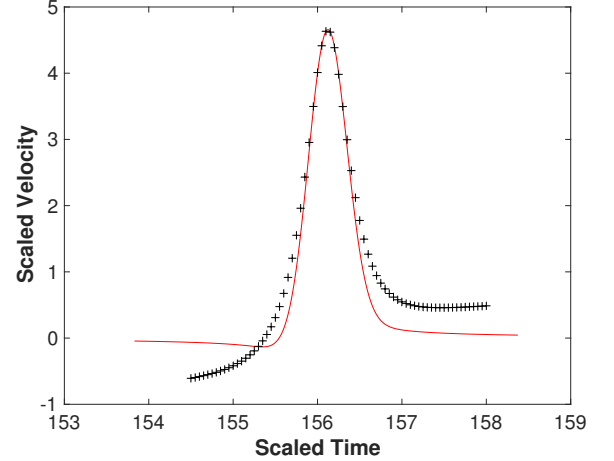

FIG. 14. Expanded view of pulse indicated by red arrow in Fig. 13. Solid red curve is the prediction of Eq. (39) and discrete symbols correspond to the numerical solution.

particle experiences relatively long periods of adiabatic balance between the slow, external force and the heat bath, during which the near-stationary conditions

$$\Gamma = A \sin(w\tau), \quad u^2 = 1 + Aw \cos(w\tau), \qquad (37)$$

are well satisfied. But, sharp, transient transfers of energy from the reservoir are triggered during which the particle acquires several times the thermal energy. The behavior is illustrated in Fig. 13 in which the temporal evolution of the scaled velocity is shown for a particle with initial scaled velocity $u(\tau = 0) = 0.1$, and
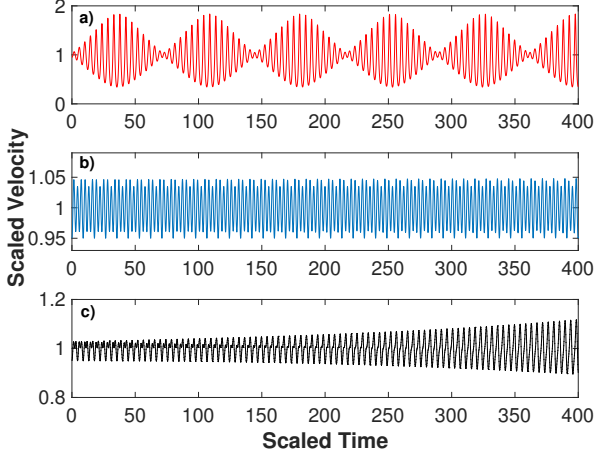
FIG. 15. Illustration of thermal resonance for a particle with $u(\tau = 0) = 0.95$. The three panels display the time evolution of the velocity for the same scaled amplitude of the external force, $A = 0.05$, but each corresponds to a different driver frequency. The red curve in the top panel corresponds to the fundamental resonance, $w = w_0 = \sqrt{2}$, the blue curve in the middle panel to an off-resonance frequency, $w = 1.5w_0$, and the black curve in the bottom panel to the second harmonic, $w = 2w_0$. A is the scaled amplitude, defined following Eq. (10), and w is the scaled frequency.

$A = 1.95$, $w = 0.09$. The nearly flat portions of the velocity curve correspond to the adiabatic behavior described by Eq. (37). The sharp pulses, reminiscent of avalanche events, are well-resolved numerically, with each encompassing several hundred computation steps and verified by using different, stiff differential-equation solvers. The pulse width is approximately about one-half of the period associated with a pure thermal orbit (of the type illustrated in Fig. 1). The shape of individual pulses can be captured by a model that assumes that over the small time interval, centered at $\tau = \tau_p$, the force is constant, of strength F_p, and the scaled damping coefficient rises linearly, i.e., locally

$$\frac{du}{ds} = F_p - asu, \text{ with } s = \tau - \tau_p, \quad (38)$$

which has a closed-form, analytic solution in terms of the imaginary error function $erfi$,

$$u = F_p \sqrt{\frac{\pi}{2a}} \exp\left(-\frac{as^2}{2}\right) erfi\left(\sqrt{\frac{a}{2}}s\right)$$
$$+ C \exp\left(-\frac{as^2}{2}\right), \quad (39)$$

with C a constant, representing the contribution from the homogeneous solution. Fig. 14 shows a comparison of the prediction given by Eq. (39), for suitable parameters, and the pulse identified by the arrow in Fig. 13, which is now shown in an expanded time-scale. For completeness, it should be mentioned that the near-adiabatic behavior,
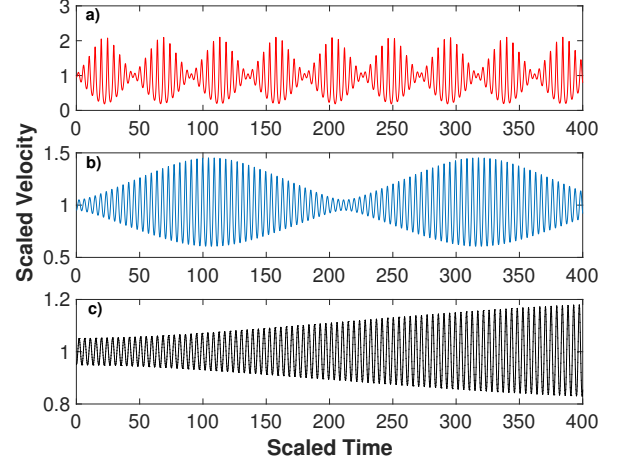

FIG. 16. Temporal evolution of the velocity for external forcing at the fundamental resonance, $w = w_0 = \sqrt{2}$, of a particle with $u(\tau = 0) = 0.95$, as in Fig. 15. Each panel corresponds to a different amplitude of the driving force. The red curve in the top panel a) is driven at $A = 0.1$ the blue curve in the middle panel b) at $A = 0.01$, and the black curve in the bottom panel c) at $A = 0.001$. A is the scaled amplitude, defined following Eq. (10), and w is the scaled frequency.

typified by Fig. 13, requires that the scaled amplitude of the external force be sufficiently large to overcome the zero-order, energy exchange with the reservoir. For the case shown in Figs. 13 and 14, $A \geq 0.5$ is necessary.

The thermal resonance suggested by Eq. (35) is illustrated in Fig. 15 for a particle with initial scaled velocity $u(\tau = 0) = 0.95$. The three panels display the time evolution of the velocity for the same scaled amplitude of the external force, $A = 0.05$, but each corresponds to a different driver frequency. The red curve in the top panel corresponds to the fundamental resonance, $w = w_0 = \sqrt{2}$, the blue curve in the middle panel to an off-resonance frequency, $w = 1.5w_0$, and the black curve in the bottom panel to the second harmonic, $w = 2w_0$. It is seen that driving at the second harmonic causes the amplitude to grow secularly, while driving at $w = 1.5w_0$ does not. Driving at the fundamental frequency is seen to result in relatively large velocity increases, comparable to the thermal velocity $\overline{v}$ (note the numerical scale is larger in the top panel). But the time series shows periodic saturations in the secular growth caused by energy loses to the heat bath when the velocity starts to deviate significantly from $\overline{v}$. To better appreciate the nature of this saturation, Fig. 16 shows the temporal evolution of the velocity, for driving at the fundamental resonance, $w = w_0 = \sqrt{2}$, but each panel now corresponds to a different amplitude of the driving force. The red curve in the top panel is driven at $A = 0.1$, the blue curve in the middle panel at $A = 0.01$, and the black curve in the bottom panel at $A = 0.001$. It is seen that at the lowest amplitude the velocity grows linearly in time, while at the larger amplitudes the thermal saturation comes into play, with the

consequence that driving at larger amplitude results in shorter intervals of departure from thermal equilibrium. Note that the velocity scale is different in the three panels, and also that all the cases are in the regime in which the average-power transfer is zero, i.e., $A < \sqrt{2}w$.

V. V. CONCLUSIONS

This study provides insight into the basic issue of how a classical particle behaves when it is simultaneously subjected to the competing tendencies of coherent driving by a sinusoidal force, and coupling to a heat bath. The perspective emphasized is that of deterministic dynamics, which is implemented by explicitly using a classic Nosé-Hoover thermostat. The value of the information obtained by this exercise is that it illustrates the underlying dynamics that is averaged over, masked by suitably chosen probability distribution functions, in the stochastic studies of such a generic situation. The results found in the present study are also useful for gaining insight into complex nonlinear problems in which a piece of the system, composed of deterministic elements, is modeled as a heat bath, as may arise in turbulence models and computer simulations.

The major feature identified in this study is the key role played by the ratio of the average oscillatory velocity to the thermal velocity, i.e., $F/\sqrt{2}m\overline{v}\omega$. It is found that, independently of the coupling strength to the thermostat, average power can only be extracted from the sinusoidal force when the oscillatory velocity exceeds the thermal velocity. It has been concluded from this property that candidate heat baths whose temperature is raised solely through the application of a sinusoidal force (e.g., radio-frequency heating), reach, in a finite time, a unique final temperature determined by the force parameters. It would be interesting to identify experimental situations, perhaps in nano-scale systems, biological environments, or microplasmas, where related issues could be studied. Other features explored in the present work, such as the combined application of AC+DC forces, could also lead to features worth exploring in the laboratory.

The transition boundary separating the two domains of power transfer has been found to define a wealth of chaotic dynamics that may be exploited for useful applications in other studies. As an example, a recent study [20] has used this region to construct chaotic versions of deterministic thermostats that better approximate the behavior of a heat bath.

In summary, new insights have been gained from a deterministic perspective on a generic topic of broad interest. More extensive studies of similar situations to those explored in this manuscript, but using other thermostat models, seem worth pursuing.

VI.   ACKNOWLEDGMENTS

[1] V. B. T. Speck, L. Helden, U. Seifert, and C. Bechinger, Phys. Rev. Lett. **96**, 070603 (2006).

[2] H. A. Kramers, Physica **7**, 284 (1940).

[3] P. Jung and P. Haenggi, Phys. Rev A **41**, 2977 (1990).

[4] I. A. Goychuck, E.G. Petrov, and V. May, Chem. Phys. Lett. **253**, 428 (1996).

[5] F. Douarche, S. Joubaud, N. B. Garnier, A. Petroysan, and S. Ciliberto, Phys. Rev. Lett. **97**, 140603 (2006).

[6] R. Van Zon and E. G. D. Cohen, Phys. Rev. Lett. **91**, 110601 (2003).

[7] J. D. Bao, Y. Abe, and Y. Z. Zhuo, Physica A **277**, 127 (2000).

[8] R. Guantes and S. Miret-Artes, Phys. Rev. E **67**, 046212 (2003).

[9] D. E. Liu, A. Levchenko, and R. M. Lutchyn, Phys. Rev. B **95**, 115303 (2017).

[10] K. Sacha and J. Zakrzewski, Rep. Prog. Phys. **81**, 016401 (2018).

[11] S. Nosé, J. Chem. Phys. **81**, 511 (1984).

[12] Wm. G. Hoover, *Computational Statistical Mechanics*, Elsevier, Amsterdam (1991).

[13] D. J. Evans and G. P. Morris, *Statistical Mechanics of Nonequilibrium Liquids*, Academic Press, New York (1990).

[14] G. P. Morris and C. P. Dettman, Chaos **8**, 321 (1998).

[15] G. J. Martyna, M. L. Klein, and M. Tuckerman, J. Chem. Phys. **97**, 2635 (1992).

[16] J. Lei and M. C. Mackey, Phys. Rev. E **84**, 041105 (2011).

[17] M. Esposito and T. Monnai, J. Phys. Chem. B **1115**, 5144 (2011).

[18] M. Tarnopolski, Physica A **461**, 662 (2016).

[19] L. Zunino, F. Olivares, A. F. Bariviera, and O. A. Rosso, Phys. Lett. A **381**, 1021 (2017).

[20] G. J. Morales, Phys. Rev. E **97**, 032203 (2018).